Available online at www.sciencedirect.com
SCIENCE DIRECT
Journal of Solid State Chemistry 179 (2006) 1602–1609
JOURNAL OF SOLID STATE CHEMISTRY
www.elsevier.com/locate/jssc

Effects of Al-doping on the stabilization of monoclinic $LiMnO_2$

Zu-Fei Huang, Chun-Zhong Wang, Xing Meng, Deng-Pan Wang, Gang Chen*

Department of Materials Science, College of Materials Science and Engineering, Jilin University, Changchun 130012, PR China

Received 4 October 2005; received in revised form 7 February 2006; accepted 12 February 2006
Available online 6 March 2006

Abstract

Electronic structures of monoclinic $LiMnO_2$ and $LiMn_{0.9375}Al_{0.0625}O_2$ with ferromagnetic (FM) and antiferromagnetic (AF) ordering have been investigated by ab initio calculation within spin-polarized generalized gradient approximation method. An Al-doping induced complicated AF configuration has been calculated to be the ground state, which suggests a robust Al-doping effect on the magnetic and electronic structures of the monoclinic $LiMnO_2$. The calculated Mulliken population analyses and partial density of states of Mn-3*d* and O-2*p* reveal that a single Al dopant stabilizes its six nearest-neighbor Mn ions in their respective octahedral sites, thereby hindering the migration of Mn ions into the interlayer Li sites during the Li intercalation–deintercalation and therefore improving both the structural stability and the electrochemical performance of the material. Additionally, it is found out that the Al-doping can decrease the JT effect and increase the intercalation voltage. The Al-doping-induced negative formation energy indicates that 6.25% Mn ions in monoclinic $LiMnO_2$ can be substituted stably by Al ions, to which the equilibrium but not metastable phase of monoclinic $LiMn_{0.9375}Al_{0.0625}O_2$ can be attributed.
© 2006 Elsevier Inc. All rights reserved.

Keywords: Monoclinic $LiMnO_2$; First-principles calculation; Electronic structures; Doping effect; Stabilization

1. Introduction

Monoclinic $LiMnO_2$ (space group $C2/m$, hereafter denoted as m-$LiMnO_2$) was first synthesized by ion exchange from α-$NaMnO_2$ in 1996, and it is thought as one of the most promising materials to replace $LiCoO_2$, the current standard cathode material in commercial Li-ion rechargeable batteries [1–9]. Unfortunately, this material transforms irreversibly to a spinel-like form upon charge–discharge cycles, leading to unacceptable capacity loss [3–9]. Because of the same ABC close-packed oxygen stacking sequence in both the monoclinic and spinel structures, such a transformation is easy to be realized by migrating only one-fourth of all Mn ions into the interlayer Li sites and moving the Li ions into the tetrahedral sites, however, without breaking the oxygen framework [3,4]. Additionally, ion-exchange reaction seems unsuitable for commercialization because it takes a long time and the products possess undesirable stoichiometries with water and protons as impurities [5,6].

For these cases, numerous attempts have been carried out to enhance the structural stability of m-$LiMnO_2$, which reveals that the partial substitution of Mn ions with other metal ions is quite effective [5–9]. Among these dopants, Al has attracted special attention because it is nontoxic, inexpensive, light and abundant in nature [1b]. Furthermore, m-$LiMn_{1-x}Al_xO_2$ can be prepared directly from a solid-state reaction at high temperature where pure $LiMnO_2$ always crystallizes in the thermodynamically stable, orthorhombic structure (*Pmnm*, o-$LiMnO_2$) [7–9]. Thus m-$LiMn_{1-x}Al_xO_2$ is synthesized as an equilibrium rather than a metastable phase, which leads to more ideal cation ordering and better crystallization compared to that of the low-temperature stabilized form of m-$LiMnO_2$, as revealed by its sharper diffraction peaks. Attractive electrochemical properties including high capacity and extended cycling stability have also been achieved in m-$LiMn_{1-x}Al_xO_2$ [7–9].

Considering the fact that the electrochemical properties of an intercalation material are linked strongly to its crystal and electronic structures, it is quite important to elucidate the effect of Al-doping on the chemical bonding and electronic structures of m-$LiMnO_2$ and thereby to

*Corresponding author. Fax: +86 431 5168446.
E-mail address: gchen@jlu.edu.cn (G. Chen).

0022-4596/$ - see front matter © 2006 Elsevier Inc. All rights reserved.
doi:10.1016/j.jssc.2006.02.016

understand the mechanism responsible for the improvement in electrochemical properties. First-principles calculations have been proved to be very effective to investigate lithium transition metal oxides [4,10,11]. Based on the total energy calculations, generalized gradient approximation (GGA) has been found vital to capture the subtle effects of Jahn–Teller (JT) distortion in lithium manganese oxides [10], and 25% Al-doped *m*-$LiMnO_2$ has been found to have lower energy than that in the orthorhombic structure [11]. However, 5–7% Al-doping is the best ratio in experiments [7–9], and we are not aware of any detailed reports on the electronic structures of *m*-$LiMn_{1-x}Al_xO_2$ compared to *m*-$LiMnO_2$. Therefore, in this work we present ab initio calculations within spin-polarized GGA-PW91 (GGS-PW91) [12] on undoped and 6.25% Al-doped *m*-$LiMnO_2$.

2. Computational methods

Calculations were performed with the CASTEP code, which implemented the GGS of density-functional theory in the ultrasoft pseudopotential representation, with a plane-wave cutoff as 400 eV [12]. The initial crystal model was built based on the experimental data but neglecting the about 10% Li/Mn site disorder [1a]. The unit cell containing two formula units was fully relaxed by geometry optimization to adjust the ionic positions and the lattice parameters until the self-consistent field (SCF) convergence per atom, tolerances for total energy, root-mean-square (RMS) displacement of atoms, RMS force on atoms and RMS stress tensor were less than 2×10^{-6} eV, 2×10^{-5} eV, 0.001 Å, 0.05 eV/Å, and 0.5 GPa, respectively. Because the magnetic structure of *m*-$LiMnO_2$ has not been well understood experimentally yet [13–16], both ferromagnetic (FM) and antiferromagnetic (AF) spin ordering were calculated. Then the 6.25% Al-doped *m*-$LiMnO_2$ supercell was built from $2\times2\times2$ optimized unit cells by replacing the body central Mn with Al. Owing to the restriction of computational resources and the estimated small structural effect induced by the small Al-doping of 6.25%, the FM and AF supercells were not relaxed but constructed directly by the optimized FM and AF unit cells of undoped *m*-$LiMnO_2$, respectively, where the AF ordering was not assigned artificially but the computer was let to choose automatically by fixing the net spin in the supercell as 4, the number of the unpaired electrons in a high-spin Mn^{3+} ion. In fact, a lot of previous publications in the field of ab initio calculation have showed that relaxation is not always necessary and neglecting the relaxation is a general operation, especially when the doping (or Li-deintercalation) ratio is not large (see Refs. [13,17,21–23,26]). Requested *k*-point spacing was set as 0.05 $Å^{-1}$, which corresponded to 32 *k*-points for *m*-$LiMnO_2$ and 8 *k*-points for 6.25% Al-doped *m*-$LiMnO_2$ in the irreducible Brillouin zone generated by the Monkhorst-Pack scheme.

3. Results and discussion

For *m*-$LiMnO_2$, the experimental cell parameters are $a=5.4387$ Å, $b=2.8086$ Å, $c=5.3878$ Å and $\beta=116.006^\circ$ [1a]. With full relaxation, the calculated values are $a=5.5339$ Å, $b=2.8618$ Å, $c=5.4562$ Å, $\beta=116.664^\circ$ for the FM solution, and $a=5.3956$ Å, $b=2.8707$ Å, $c=5.3760$ Å, $\beta=114.778^\circ$ for the AF solution. The consistence between the experimental and calculated data reveals the validity of our calculations. The difference between these two solutions is obviously resulted from the different magnetic interactions. As to the deviation from the experimental data, it can be mainly ascribed to the fact that the experimental structure has about 10% Li/Mn site disorder [1a], but our calculated structures have fully ordered Li/Mn site distribution. Because *b* measures the nearest Mn–Mn distance, when an Li^+ ion replaces an Mn ion in the Mn site, the electrostatic repulsion along *b*-axis reduces greatly because of the much less charges of Li^+ ion compared to the Mn^{3+} ion. Therefore, the experimental *b* constant is smaller than the calculated ones.

In order to investigate the effects of Al-doping on the chemical bonding, we performed the Mulliken population analyses. It is found that Al-doping has divided the Mn and O ions into two and three types, respectively. While for the Li ions, Al-doping does not bring any distinct changes. The results are listed in Table 1, where the suffix I, II or III simultaneously denotes the first, second or third nearest-neighbor ions to the Al ion, and the remainder Li, Mn and O ions in the supercells can be classified as Li_I, Mn_{II} and O_{III} ions, respectively. These assignments are also shown in Fig. 1, where the AlO_6 and an edge-shared LiO_6 octahedron are plotted with blue sticks, and the six O ions belonging to an edge-shared $Mn_{II}O_6$ octahedron are connected to the central Mn_{II} ion by half-blue-half-magenta sticks. One can note that the O_I/O_{II} ions locate at the equatorial/axial vertexes of the elongated AlO_6 octahedron and each AlO_6 octahedron has six edge-shared, elongated MnO_6, i.e. two Mn_IO_6 and four $Mn_{II}O_6$ octahedrons. The Mn_IO_6 octahedron shares two equatorial vertexes, i.e. two O_I ions while the $Mn_{II}O_6$ octahedron shares a side edge, i.e. an O_I ion and an O_{II} ion with the AlO_6 octahedron. For the O_{III} ion, it is the equatorial ion of the elongated $Mn_{II}O_6$ octahedron, too. Owing to the lack of relaxation, the Al dopant is fixed at an optimized Mn site and hence the Mn–O distances are equal to the Al–O distances.

As shown by the magnetic moments (*M*) at Mn sites, FM or AF ordering has been reproduced successfully. For simplicity, we can assume that the Curie–Weiss effective moment (μ_{eff}) is dependent only on the transition ions' average spin (*S*) by following the equations $\mu_{eff}=2\sqrt{S(S+1)}$ and $S=M/2$ [17]. Then μ_{eff} 4.61 μ_B and 4.63 μ_B are obtained for undoped FM and AF solutions, respectively, in good agreement with the experimentally observed value of 4.59 μ_B [14]. According to the redistribu-

Table 1
Calculated net charges (Q) and magnetic moments (M) of different ions in the FM and AF m-$LiMn_{0.9375}Al_{0.0625}O_2$ compared to m-$LiMnO_2$ (given in the brackets), together with their respective distance to the Al ion (D) and the corresponding bond overlap population (OP)

Ion types		Li_I	Mn_I	Mn_{II}	O_I	O_{II}	O_{III}	Al
FM	Q	+1.04 (+1.04)	+0.60	+0.58 (+0.58)	−0.95	−0.85	−0.81 (−0.81)	+1.23
	M (μ_B)	0.00 (0.00)	+3.72	+3.72 (+3.72)	+0.10	+0.06	+0.14 (+0.14)	+0.02
	D (Å)	2.8851	2.8618	3.1150	1.9683	2.3678	3.6550	—
	OP	−0.09	−0.63	—	+0.41	+0.18	—	—
AF	Q	+1.04 (+1.05)	+0.59	+0.57 (+0.57)	−0.94	−0.85	−0.81 (−0.81)	+1.22
	M (μ_B)	0.00 (±0.02)	−3.72	±3.68 (±3.74)	±0.07	±0.03	±0.10 (0.00)	−0.04
	D (Å)	2.9026	2.8707	3.0559	1.9693	2.3267	3.5748	—
	OP	−0.09	−0.63	—	+0.40	+0.19	—	—

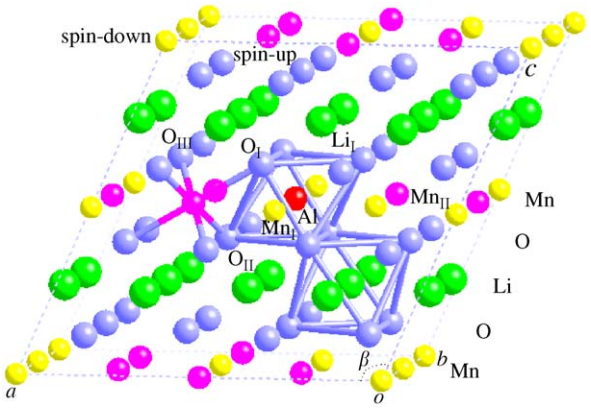

Fig. 1. Geometric and magnetic structures of the AF Al-doped supercell, where the spin-up and spin-down Mn ions are denoted by the yellow and magenta balls, respectively.

tion of M with Al-doping, it is obvious that AF solution has been influenced more compared to FM solution. Without Al-doping, the spin alignment of Mn ions forms FM chains along the b-axis with AF interchain correlation in the ab plane but FM stacking along the c-axis, similar to Singh's AF2 magnetic structure [13]. However, with doping, the magnetic configuration of the AF supercell becomes more complex as shown in Fig. 1, which can be viewed as some kind of the combination of Singh's AF2 and AF3 (AF chains along the b direction with two of the other four Mn neighbors AF and two FM) configurations. Here we would like to point out that such a configuration is the computer's automatic choice but not assigned artificially. Therefore, this configuration seems to respond to a favored stability over many other collinear AF, including the AF2 and AF3 spin arrangements. Although it is not clear yet why such an alignment is advantaged in energy and it needs more investigation, the transformation in the AF configuration reveals obviously that the effects of Al-doping are not limited in the doped Mn layer and the interlayer interaction is existent and important. Experimentally, it has been reported that Co doping in the perovskite $LaMnO_3$ transforms the AF host to an FM structure [18]. Of course, one should recall that our most stable AF configuration is obtained from a non-relaxed calculation, so relaxing the structure might stabilize a different ground state. Nevertheless, as expatiated in Section 2, it seems reasonable that this different ground state might be closely related to the one found without relaxation.

For the net charges (Q), the values for Mn and O ions always deviates largely from their formal charges, implying that the Mn–O bonds are still strongly covalent as proven by the positive values of bond overlap population (OP), a parameter to directly measure the strength of a bond's covalent/ionic interaction by a positive/negative value. Nevertheless Al-doping has enhanced the ionicities of Mn and O ions around it, as revealed by the larger Q values compared to those in m-$LiMnO_2$ (see Table 1). Since each octahedron has six edge-shared octahedrons in this structure (see Fig. 1), the enhanced ionicities of O ions have strengthened the Mn–O bond interactions in the six MnO_6 octahedrons, which results in the stabilization of the six Mn ions in their respective octahedral sites. Additionally, the much larger Q of Al ion indicates its more fixation in the octahedral site than that of Mn ion. Experimentally, it has been found that the superior electrochemical performance of Cr-doped m-$LiMnO_2$ can be attributed to the shortening of Mn–O bonds, leading to the stabilization of Mn ions in the octahedral sites and thereby hindering their migration into the interlayer Li sites during cycling [19], while the slight improvement of Ni-doped m-$LiMnO_2$ can be owed to the incomplete fixation of the Ni ion in the octahedral site accompanied by the displacement of the Mn ions [20]. Therefore, doping only one Al ion has enhanced the fixation of itself and its six nearest-neighbor Mn ions (Mn_I and Mn_{II}) in the octahedral sites, which can hold back their migration into the interlayer Li sites during cycling and thereby improve the material's stabilization and electrochemical properties significantly. Our conclusion agrees well with the experimental facts that doping of as little as 5% Mn by Al has realized the synthesis of m-$LiMnO_2$ under equilibrium conditions and attractive electrochemical performance of m-$LiMn_{1-x}Al_xO_2$ compared to m-$LiMnO_2$ has been achieved [7–9]. Additionally, the more ionized O ions indicate that Al-doping has

transferred more electrons to them and Li–O interactions have been strengthened. According to the previous reports [21–23], this can increase the material's intercalation voltage because the strengthened Li–O interactions demand more energy for the Li-deintercalation.

It is clear now that the Al dopant has enhanced the fixation of its six Mn neighbors in their respective octahedral sites. However, the effect is not isotropic and is strongest on the Mn_I ions, which locate with Al along the same *b*-axis as shown by the *Q* values for Mn ions (see Fig. 1 and Table 1). Because the Mn and Al ions on the *b*-axis have much more positive net charges, the electrostatic repulsion is much larger along the *b*-axis than that along the *a*-axis, which will reduce the *a*/*b* ratio. In experiments and theoretical calculations, it has been found that *a*/*b* magnitude is related to the average degree of distortion in the octahedrons of O ions around the Mn ions, and the reduction in the magnitude means that the JT effect has been decreased [8,16,23]. Therefore, besides by diluting the number of JT active high-spin Mn^{3+} sites, Al-doping can decrease the JT effect by enhancing the ionicities of nearest-neighbor Mn ions. It has been suggested that the decrease in the JT distortion upon cation substitution can contribute partially to the cycling stability [16,19].

Fig. 2 shows the calculated total density of states (DOS) around the Fermi level (E_F) without and with Al-doping for the FM and AF solutions. It is evident that the spin-up and spin-down states in panel (b) are nearly identical, displaying the unique character of the electronic structures for AF ordering. At a glance, one can note that the main characters of the DOS are maintained with Al-doping. For example, the profiles of DOS can be divided into about four portions: the states extending from about −6.5 eV to −2.5 eV are mainly derived from the six O-2*p* orbitals of two O ions per formula unit, and the higher occupied states from about −2.5 eV to the E_F are assigned in turn to the half-filled t_{2g} and e_g bands of the five Mn-3*d* orbitals with a ligand field splitting between them, while the conduction bands extending to about 4 eV are composed of the remainder t_{2g} and e_g states [22–24]. Because of JT effect, the e_g bands in one spin species split into the highest valence bands (d_{z^2} orbital) and the lowest conduction bands ($d_{x^2-y^2}$ orbital) [23,24], responding to the semiconducting character of these materials as marked in Fig. 2. Such assignments are confirmed by the partial DOS (PDOS) shown in Figs. 3 and 4, where for simplicity and clarity, one-ion type as defined in Table 1 is represented by only one appointed ion's PDOS. Nevertheless, one should keep in mind that one-ion type always has many ions, whose spin characters may be antiparallel in the AF solution (see Table 1 and Fig. 1).

However, noticeable changes with Al-doping can also be observed. Firstly, with careful observation, one can find that the peak of occupied spin-up e_g states (d_{z^2}) in Fig. 2(b) is stronger than that of the spin-down states and there is also a slight exchange splitting between the spin-up and spin-down states, indicating the net spin of 0.25/f.u. induced by the 1/16 Al-doping in the AF supercell.

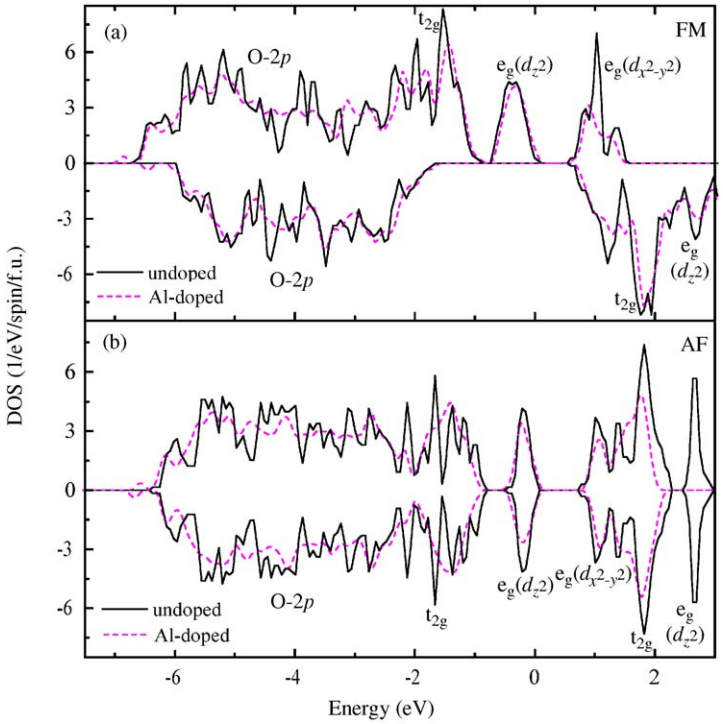

Fig. 2. Calculated total density of states (DOS) around E_F (0 eV) without (solid line) and with (dash line) Al-doping for the FM (a) and AF (b) spin ordering. Spin-up/down states are plotted along the positive/negative ordinate.

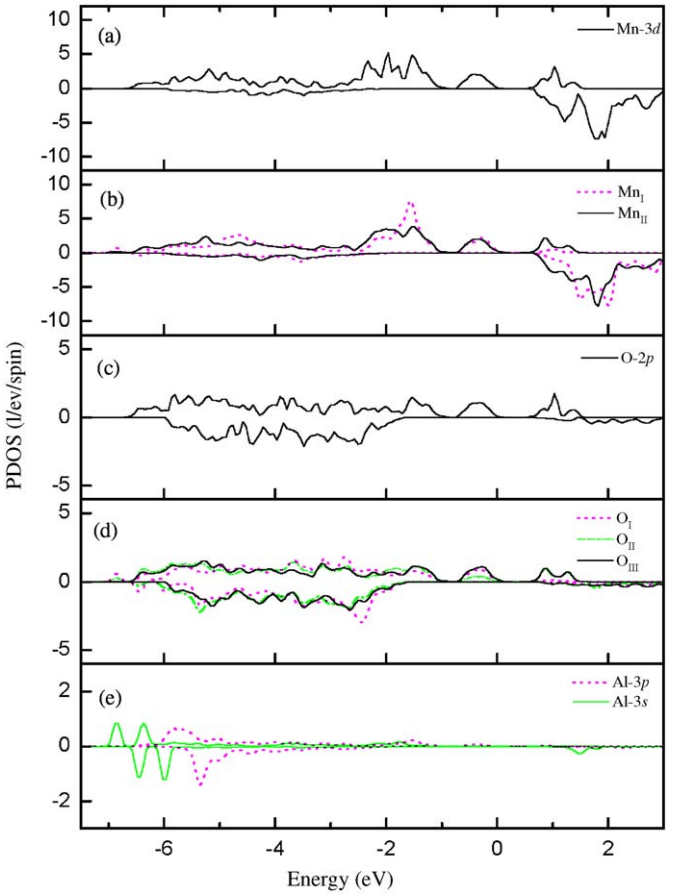

Fig. 3. Partial density of states (PDOS) around E_F (0 eV) of Mn-3*d*, O-2*p* and Al-3*p*, 3*s* without (a, c panels) and with (b, d and e panels) Al-doping for the FM solution. When comparing contributions of different states, note the different scale of panels.

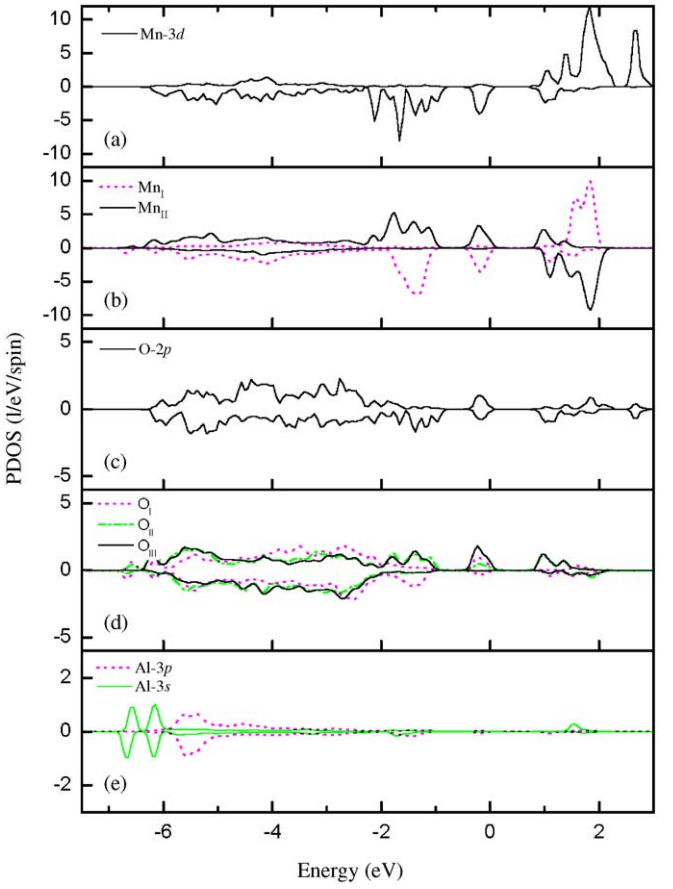

Fig. 4. PDOS around E_F (0 eV) of Mn-3*d*, O-2*p* and Al-3*p*, 3*s* without (a, c panels) and with (b, d and e panels) Al-doping for the AF solution. Note the different scale of panels.

Secondly, the DOS becomes more flat over the whole energy range. Thirdly, new bands appear from about −7 eV to −6 eV. Combining Figs. 3 and 4, it is clear that they are introduced mainly by Al-3*p*, 3*s* orbitals. Interestingly, the Al-3*s* states show an unusual splitting. In order to find out what actually drives this splitting, we have performed another calculation on the *m*-$LiAlO_2$ that adopts the same structure as FM *m*-$LiMnO_2$ and FM supercell. This time, no splitting in the Al-3*s* PDOS is found. Therefore, it is reasonable to conclude that the splitting is mainly resulted from the Al–Mn interaction. Such significant residuals of Al-3*p*, 3*s* states reflect strong covalent interaction between Al and O ions, and demand accompanying O-2*p* states in the same energy range, consistent with the values of *Q* and OP listed in Table 1 and the O-2*p* PDOS shown in Figs. 3 and 4. The appearance of new O-2*p* states in the lower energy position can enhance the interaction between O ions and cations, thereby stabilizing the structures and leading to a higher intercalation voltage [21–23]. Fourthly, the Mn-3*d* bands, especially t_{2g} bands get narrower and their separation from the O-2*p* bands becomes more evident; a slight increase in the separation between t_{2g} and e_g states, the ligand field splitting, can also be detected. It has been found that the Mn-3*d*, especially t_{2g} bandwidth is controlled by the Mn–Mn interaction [22]. Thus, the narrower Mn-3*d* bandwidth with Al-doping reveals that the interaction between Mn ions has been weakened, which consists with the increase in the electrostatic repulsion caused by the enhanced ionicities of Mn ions, as reflected by the *Q* values listed in Table 1. As for the separation between O-2*p* and Mn-3*d* bands, it reflects the ionic character in the chemical bonding between O and Mn ions [22,23,25]. Therefore, the larger separation means that Al-doping has increased the ionic character and interaction of Mn–O bonds, consistent with the increase in both the *Q* values for O and Mn ions; in a similar way, the enlarged splitting between the t_{2g} and e_g states arises from the enhanced ligand field caused by the increase in the ionicity of O ions with Al-doping. Lastly, the insulating gap is enlarged by an order of about 0.1 eV (increasing from 0.56 eV to 0.68 eV for FM solution and from 0.79 eV to 0.92 eV for AF solution with Al-doping by ruling out the smearing). All these changes indicate that Al-doping has surely stabilized the structures effectively.

Besides the changes in the total DOS, PDOS can give additional information. From Figs. 3 and 4, significant amounts of Mn-3*d* states are found in the energy range of

O-2p bands, and the mixing of O-2p states in the Mn-3d bands, particularly in the e_g bands is also notable, which supplies the direct evidence for the strong covalent interaction of Mn–O bonds and reflects the bonding character of O-2p bands and the anti-bonding character of e_g bands, analogous to other lithium transition-metal oxides and very crucial to the cathode material's electrochemical properties [1b,10,13,22–27]. In the simplified diagrams of ionic molecular-orbital theory, the t_{2g} bands are non-bonding character [22,26]. Practically, however, because of the presence of other states such as Li-1s, 2s, Mn-4s, 4p and O-2s (not shown in Figs. 3 and 4 for their negligible contributions in this energy range) and the translational invariance, they exhibit some degree of bonding character as shown by the emergence of O-2p states in their energy range [26]. Because of the JT effect, the two orbitals composing the e_g states have been split, making the d_{z^2} orbital occupied and leaving the $d_{x^2-y^2}$ orbital empty (see Figs. 2–4). Because of the about 4 eV exchange splitting in the Mn-3d states, one of the two spin species, i.e. the whole spin-up or spin-down states, has been lifted up above the E_F. Consequently, the Mn-3d PDOS present vividly a high-spin Mn ion with the electronic configuration $t_{2g}^3 e_g^1$. That is to say, the Al dopant adopts the +3 oxidation state and does not change the oxidation states of Mn^{3+}. At the same time, such a high-spin state makes the hybridization between Mn-3d and O-2p states spin dependent, which leads to the exchange splitting in the O-2p states and the reduction of the spin moment on Mn sites considerably from the nominal Hund's rule value, consistent with Singh's report [13] and the M values listed in Table 1.

Comparing the PDOS without and with Al-doping, we can find distinct changes on the Mn_I, O_I and O_{II} ions, where their e_g majority states all have been attenuated significantly in addition to the much narrower t_{2g} bands of Mn_I ions as discussed above. For comparison numerically, we have calculated the integration intensities of the majority states for the d_{z^2} and $d_{x^2-y^2}$ as well as the e_g (i.e. their sums) orbitals of the Mn and O ions. The results are listed in Table 2. It can be found that the e_g states of the Mn_I, Mn_{II} and O_I, O_{II} ions have decreased assuredly. As mentioned above, the O_I, O_{II} and O_{III} ions also belong to the AlO_6 octahedron's six edge-shared, elongated MnO_6, i.e. two Mn_IO_6 and four $Mn_{II}O_6$ octahedrons (see Fig. 1). Additionally, the e_g states are anti-bonding character, so their decrease indicates that Al-doping has enhanced considerably the bonding, i.e. the interaction between the Mn_I, Mn_{II} and their surrounding O, i.e. O_I, O_{II}, O_{III} ions [22,27]. Here we would like to point out that the attenuated e_g states with Al-doping result in the enhanced ionic character of the Mn–O bonds, because the e_g states are anti-bonding and mainly composed of the Mn-3d d_{z^2} and $d_{x^2-y^2}$ orbitals. Therefore, for the Mn ions, less e_g states reveal more Mn-3d electrons have transferred to O ions; at the same time, the decrease in the e_g part of the O-2p PDOS indicates more occupied O-2p orbitals [27]. Both evidences show more ionized Mn and O ions with Al-doping, consistent with our conclusion above.

Table 2
Integration intensities of the majority states for the d_{z^2} and $d_{x^2-y^2}$ as well as the e_g (i.e. their sums) orbitals of the Mn and O ions without (Mn and O columns) and with (Mn_I, Mn_{II} and O_I, O_{II}, O_{III} columns) Al doping

Orbital		Mn	Mn_I	Mn_{II}	O	O_I	O_{II}	O_{III}
FM	d_{z^2}	*0.921*	0.958	0.912	*0.490*	0.395	0.176	0.497
	$d_{x^2-y^2}$	*0.916*	0.156	0.799	*0.479*	0.043	0.387	0.410
	Total (e_g)	*1.837*	1.114	1.711	*0.969*	0.438	0.563	0.907
AF	d_{z^2}	*0.950*	0.978	0.950	*0.429*	0.367	0.154	0.508
	$d_{x^2-y^2}$	*0.955*	0.921	0.927	*0.502*	0.112	0.455	0.483
	Total (e_g)	*1.905*	1.899	1.877	*0.931*	0.479	0.609	0.991

From Figs. 3 and 4 and Table 2, however, one can note that the enhanced interaction is not symmetric but has preferred orientation as revealed by the asymmetric attenuation in the two orbitals of e_g states, where the attenuation take places mainly in the $d_{x^2-y^2}$ states and also in the d_{z^2} states for the O_{II} ions. These preferred orientations reflect the structural features of the monoclinic symmetry. In the elongated MnO_6 octahedron, the $d_{x^2-y^2}$ orbital points to the four equatorial vertexes along the X and Y directions while d_{z^2} orbital extends along the Z direction of the octahedral inner coordinates [22–24,27]. For the two Mn_IO_6 octahedrons, each of them shares two equatorial vertexes, i.e. two O_I ions with the AlO_6 octahedron. Because the e_g states of Mn_I and O_I ions mainly decrease in the $d_{x^2-y^2}$ orbital, it is natural that the interaction between the Mn_I and O_I ions is strengthened mainly along the X and Y directions in the equatorial plane of the octahedron, thereby stabilizing considerably the Mn_I ion in its own octahedral site. For the four $Mn_{II}O_6$ octahedrons, each of them shares a side edge, i.e. an O_I ion and an O_{II} ion with the AlO_6 octahedron. That is to say, the equatorial/axial O_I/O_{II} ion in the AlO_6 octahedron becomes the axial/equatorial "O_{II}"/ "O_I" ion in the $Mn_{II}O_6$ octahedron (see Fig. 1). For the O_{III} ion, it is the equatorial ion of the elongated $Mn_{II}O_6$ octahedron, too. Therefore, although the Mulliken population analyses above show no changes with Al-doping on the ionicities of the Mn_{II} and O_{III} ions (see Table 1), the stabilization of the Mn_{II} ion in its own octahedral site is enhanced actually by decreasing the $d_{x^2-y^2}$ states of Mn_{II}, O_{II}, O_{III} ions and the d_{z^2} states of Mn_{II}, O_I ions (see Table 2). As a result, the changes in the e_g majority states of the Mn-3d and O-2p PDOS with Al-doping offer direct and strong evidences that a single Al dopant in m-$LiMnO_2$ indeed has enhanced the fixation of its six Mn neighbors in their respective octahedral sites, which can hinder the migration of Mn ions into the interlayer Li sites during cycling, thereby improving both the structural and the electrochemical stabilities [4,19,20]. This result reinforces the above conclusion simply based on the Mulliken population analyses.

Based on the calculated total energy per formula unit (E), the average intercalation voltage ($\bar{V}$), one of the most important parameters for a cathode material, can be calculated ab initio from the difference between the E values of the cathode (E_{LiMO_2}), its Li-deintercalated form (E_{MO_2}) and the anode, such as Li metal (E_{Li}) [22],

$$\bar{V} = -\frac{\Delta G_r}{(x_2 - x_1)F} \approx -\frac{E_{LiMO_2} - E_{MO_2} - E_{Li}}{e}. \quad (1)$$

In Eq. (1), ΔG_r is the change in the Gibbs free energy with the Li content in the cathode decreasing from x_2 to x_1, F is the Faraday constant and e is the elementary electric charge. Taking example for the FM solution, we have calculated that the Al-doping has indeed increased $\bar{V}$ from 4.77 to 4.85 V, in good agreement with the results above. Experimentally, an initial and a cutoff potentials of 3.3 and 4.3 V were measured, respectively [1a], indicating $\bar{V}$ should approximate 3.8 eV for m-$LiMnO_2$. Obviously, $\bar{V}$ is overestimated by about 1 eV, while it is well documented that ab initio calculations usually give an underestimation [21,22]. Although the reason for this divergence has not been clearly determined yet, according to Eq. (1), it seems to arise mainly from the non-relaxed calculation on the Li-deintercalated structure MO_2, because a full relaxation can decrease the E_{MO_2} value greatly, thereby decreasing the $\bar{V}$ value. Actually, we have found that $E_{m\text{-}MnO_2}$ is decreased indeed by 1.016 eV with full relaxation. Again, here we would like to point out that the former value (4.77 eV) is calculated from the fully relaxed m-$LiMnO_2$, while the latter (4.85 eV) is from the non-relaxed m-$LiMn_{0.9375}Al_{0.0625}O_2$. Therefore, relaxing the structure might change the absolute $\bar{V}$ value. Nevertheless, as having been elucidated above, it is reasonable to believe that the increasing trend should not be altered. But for an undoped cathode material, one should keep in mind that ab initio methods without relaxation may be unlikely to provide quantitative results, as concluded in Ref. [22].

In order to estimate directly that whether the structure of Al-doped m-$LiMnO_2$ is stable or not, the formation energy (ΔE) is calculated from E by evaluating the equation

$$\Delta E = E_{m\text{-}LiMn_{1-x}Al_xO_2} - \left[(1-x)E_{m\text{-}LiMnO_2} + xE_{m\text{-}LiAlO_2}\right]. \quad (2)$$

ΔE is calculated as -2 and -20 meV for FM and AF solutions, respectively, and the AF structures always have lower energies, 49 meV without Al-doping and 70 meV with doping, than the FM structures. The negative formation energies clearly indicates that 6.25% Al-doping in m-$LiMnO_2$ is stable indeed for both FM and AF solutions, consisting with the experiments that Al-doped m-$LiMnO_2$ is an equilibrium phase, while pure m-$LiMnO_2$ is a metastable one [7–9]. Because the AF structures always have lower energies than the FM structures, we conclude that AF interaction dominates in these structures, which agrees well with the experimental facts that large negative Weiss constants as well as the short-range AF ordering were reported for both pure m-$LiMnO_2$ and Al-doped m-$LiMnO_2$ [14,15].

Now we can give an outline of the changes in m-$LiMnO_2$ with Al-doping: The ionicities of the Mn and O ions surrounding the Al dopant are enhanced, which strengthens the interactions of the related Al–O, Mn–O, Li–O bonds and the electrostatic repulsion between the cations along the b-axis, thereby raising the stability of Al, Mn, Li ions in their own octahedral sites (O_h) and decreasing the JT distortion, respectively. Consequently, the structure is stabilized and the intercalation voltage increases with the Al-doping. In fact, according to the two-stage mechanism proposed by Reed et al. for the layered-to-spinel transformation during the electrochemical cycling [4], the more ionized Mn ions induced by the Al-doping can also stabilize this material remarkably. Through ab initio calculations, they argued that the migration of Mn ions in m-$LiMnO_2$ from their initial O_h into another O_h in the Li interlayers favors to pass through an adjacent intermediate tetrahedral site (T_d) in the Li planes, as denoted by $O_h \rightarrow T_d \rightarrow O_h$. When migrating to T_d, an accompanying charge disproportionation as $2Mn^{3+} \rightarrow Mn^{2+} + Mn^{4+}$ is necessary, where Mn^{2+} is the migrating ion because only the $+2$ oxidation state for the Mn ions is correlated with low-energy T_d occupation [4b]. Based on this mechanism as reviewed excellently in Ref. [4b] by Reed and Ceder, they suggested that substitution with fixed low-valence cations such as Al^{3+} and Mg^{2+} or more electronegative multivalent elements such as Co^{3+} and Cr^{3+} can effectively reduce the electron supply needed to form Mn^{2+} from Mn^{3+}, thereby hindering the Mn passage along $O_h \rightarrow T_d \rightarrow O_h$ type paths and forcing the Mn ions in their initial O_h. Obviously, our more oxidated Mn ions indicate that the electron supply has been reduced certainly with Al-doping. Therefore, our conclusions coincide well with theirs [4].

4. Conclusions

Using GGS method, we have calculated ab initio the electronic structures of AF and FM m-$LiMnO_2$ without and with 6.25% Al-doping. Without artificial assignments, FM and AF structures have been obtained successfully. Furthermore, Al-doping has altered the AF alignments not only in the doped but also in the next Mn layers, offering a new AF magnetic configuration and revealing that the doping effects actually are not restricted in the finite local environment around the Al dopant. The results of both Mulliken population analyses and Mn-3d as well as O-2p partial DOS reveal that a single Al dopant has strengthened the Mn–O interactions in the six MnO_6 octahedrons that share a common edge with the AlO_6 octahedron, thereby stabilizing the six Mn ions in their respective octahedral sites and improving both the structural and the electrochemical stabilities of m-$LiMnO_2$ by hindering the migration of Mn ions into the interlayer Li sites during cycling. The more ionic O ions with Al-doping have also strengthened the Li–O interactions, responding for the

higher intercalation voltage. Additionally, JT inactive Al ion has replaced a JT active Mn^{3+} ion, and the electrostatic repulsion along the *b*-axis has increased, leading to the decrease of JT effect. In the total DOS, Al-doping has smoothed the profiles of states, introduced new bands at the bottom of O-2*p* bands, narrowed the t_{2g} bands and enlarged the insulating gap as well as the separation between the Mn-3*d* and O-2*p* states. Finally, the negative formation energy proves directly that the 6.25% Al-doping *m*-$LiMnO_2$ has a stable structure. Therefore, we suggest that the synthesis of *m*-$LiMn_{1-x}Al_xO_2$ under equilibrium conditions and its improved electrochemical properties can be attributed to the great effects of Al-doping on the stabilization as summarized above.

Acknowledgments

This work was sponsored by both the Chinese Natural Science Foundation, under Grant No. 50272023, the Special Funds for Major State Basic research Project of China under Grant no. 2002CB211802 and a component part of Key Project 10411 from the Ministry of Education, China.

References

[1] (a) A.R. Armstrong, P.G. Bruce, Nature (London) 381 (1996) 499;
(b) G. Ceder, Y.-M. Chiang, D.R. Sadoway, M.K. Aydinol, Y.-I. Jang, B. Huang, Nature (London) 392 (1998) 694.
[2] F. Capitaine, P. Gravereau, C. Delmas, Solid State Ionics 89 (1996) 197.
[3] S.-J. Hwang, H.-S. Park, J.-H. Choy, G. Campet, Chem. Mater. 12 (2000) 1818.
[4] (a) J. Reed, G. Ceder, A. Van Der Ven, Electrochem. Solid-State Lett. 4 (2001) A78;
(b) J. Reed, G. Ceder, Chem. Rev. 104 (2004) 4513.
[5] Z.P. Guo, S. Zhong, G.X. Wang, G. Walter, H.K. Liu, S.X. Dou, J. Electrochem. Soc. 149 (2002) A792.
[6] P. Suresh, A.K. Shukla, N. Munichandraiah, Electrochem. Solid-State Lett. 8 (2005) A263.
[7] Y.-I. Jang, B. Huang, Y.-M. Chiang, D.R. Sadoway, Electrochem. Solid-State Lett. 1 (1998) 13.
[8] B. Ammundsen, J. Desilvestro, T. Groutso, D. Hassell, J.B. Metson, E. Regan, R. Steiner, P.J. Pickering, J. Electrochem. Soc. 147 (2000) 4078.
[9] Y.-I. Jang, Y.-M. Chiang, Solid State Ionics 130 (2000) 53.
[10] S.K. Mishra, G. Ceder, Phys. Rev. B 59 (1999) 6120.
[11] G. Ceder, S.K. Mishra, Electrochem. Solid-state Lett. 2 (1999) 550.
[12] (a) J.P. Perdew, Y. Wang, Phys. Rev. B 46 (1992) 6671;
J.A. White, D.M. Bird, Phys. Rev. B 50 (1994) 4954;
(b) Accelrys Inc., CASTEP Users Guide, Accelrys Inc., San Diego, 2001;
V. Milman, B. Winkler, J.A. White, C.J. Pickard, M.C. Payne, E.V. Akhmatskaya, R.H. Nobes, Int. J. Quant. Chem. 77 (2000) 895.
[13] D.J. Singh, Phys. Rev. B 55 (1997) 309.
[14] M. Tabuchi, K. Ado, H. Kobayashi, H. kageyama, J. Electrochem. Soc. 145 (1998) L49.
[15] Y.-I. Jang, F.C. Chou, Y.-M. Chiang, J. Phys. Chem. Solids 60 (1999) 1763.
[16] R. Prasad, B. Benedek, M.M. Thackeray, Phys. Rev. B 71 (2005) 134111.
[17] G.E. Grechnev, R. Ahuja, B. Johansson, O. Eriksson, Phys. Rev. B 65 (2002) 174408.
[18] S. Hebert, C. Martin, A. Maignan, R. Retoux, M. Hervieu, N. Nguyen, B. Raveau, Phys. Rev. B 65 (2002) 104420.
[19] S.-J. Hwang, H.-S. Park, J.-H. Choy, G. Campet, J. Phys. Chem. B 104 (2000) 7612.
[20] H.-S. Park, S.-J. Hwang, J.-H. Choy, J. Phys. Chem. B 105 (2001) 4860.
[21] (a) S. Shi, C. Ouyang, D -S. Wang, L. Chen, X. Huang, Solid State Comm. 126 (2003) 531;
(b) S. Shi, D.-S. Wang, S. Meng, L. Chen, X. Huang, Phys. Rev. B 67 (2003) 115130.
[22] M.K. Aydinol, A.F. Kohan, G. Ceder, K. Cho, J. Joannopoulos, Phys. Rev. B 56 (1997) 1354.
[23] Z.-F. Huang, X. Meng, C.-Z. Wang, Y. Sun, G. Chen, J. Power Sources (in press, available online).
[24] Y.J. Wei, X.G. Xu, C.Z. Wang, C. Li, G. Chen, Appl. Phys. Lett. 83 (2003) 1791.
[25] Y. Liu, T. Fujiwara, H. Yukawa, M. Morinaga, Solid State Ionics 126 (1999) 209.
[26] M.T. Czyżyk, R. Potze, G.A. Sawatzky, Phys. Rev. B 46 (1992) 3729.
[27] X.G. Xu, C. Li, J.X. Li, U. Kolb, F. Wu, G. Chen, J. Phys. Chem. B 107 (2003) 11648.